Mon. Not. R. Astron. Soc. **000**, 1–13 (2005) Printed 6 December 2007 (MN LATEX style file v2.2)

The IPHAS Catalogue of Hα Emission Line Sources in the Northern Galactic Plane

A. R. Witham,[1] C. Knigge,[1] J. E. Drew,[2] R. Greimel,[3,4] D. Steeghs[5,6]
B. T. Gänsicke,[5] P. J. Groot,[7] A. Mampaso[8]
[1] *School of Physics & Astronomy, University of Southampton, Highfield, SO17 1BJ, U.K*
[2] *Imperial College London, Blackett Laboratory, Exhibition Road, London, SW7 2AZ, U.K*
[3] *Isaac Newton Group of Telescopes, Apartado de correos 321, E-38700 Santa Cruz de la Palma, Spain*
[4] *Institute of Physics, University of Graz, Universitätsplatz 5, 8010 Graz, Austria*
[5] *Department of Physics, University of Warwick, Coventry CV4 7AL, U.K.*
[6] *Harvard-Smithsonian Center for Astrophysics, 60 Garden Street, Cambridge, MA 02138, USA*
[7] *Department of Astrophysics/IMAPP, Radboud University Nijmegen, P.O. Box 9010, 6500 GL, Nijmegen, The Netherlands*
[8] *Instituto de Astrofísica de Canarias, 38200 La Laguna, Tenerife, Spain*

2005 August 5

ABSTRACT

We present a catalogue of point-source Hα emission line objects selected from the INT/WFC Photometric Hα Survey of the Northern Galactic Plane (IPHAS). The catalogue covers the magnitude range $13 \leqslant r' \leqslant 19.5$ and includes northern hemisphere sources in the Galactic latitude range $-5^\circ < b < 5^\circ$. It is derived from ~ 1500 deg^2 worth of imaging data, which represents 80% of the final IPHAS survey area. The electronic version of the catalogue will be updated once the full survey data becomes available. In total, the present catalogue contains 4853 point sources that exhibit strong photometric evidence for Hα emission. We have so far analyzed spectra for ~ 300 of these sources, confirming more than 95% of them as genuine emission-line stars. A wide range of stellar populations are represented in the catalogue, including early-type emission line stars, active late-type stars, interacting binaries, young stellar objects and compact nebulae.

The spatial distribution of catalogue objects shows overdensities near sites of recent or current star formation, as well as possible evidence for the warp of the Galactic plane. Photometrically, the incidence of Hα emission is bimodally distributed in $(r' - i')$. The blue peak is made up mostly of early-type emission line stars, whereas the red peak may signal an increasing contribution from other objects, such as young/active low-mass stars. We have cross-matched our Hα-excess catalogue against the emission-line star catalogue of Kohoutek & Wehmeyer (1999), as well as against sources in SIMBAD. We find that fewer than 10% of our sources can be matched to known objects of any type. Thus IPHAS is uncovering an order of magnitude more faint ($r' > 13$) emission line objects than were previously known in the Milky Way.

Key words:
surveys – catalogues – stars: emission-line, Be – Galaxy: stellar content

1 INTRODUCTION

Large-scale Hα imaging surveys have traditionally focused on extended emission line sources, such as the nebulosities associated with areas of intense star formation. However, many interesting classes of stars also display Hα emission and, in principle, can therefore be efficiently identified in such surveys as point-source Hα-excess objects. More often than not, line emission is associated with stars in very early or very late evolutionary stages that are short-lived and relatively poorly understood. Line emission is also often associated with binaries experiencing mass transfer and accretion. The list of line-emitting classes of stars includes post-asymptotic and some asymptotic giant branch (AGB) stars, compact planetary nebulae, luminous blue variables,

hypergiants, Wolf-Rayet stars, classical Be stars, active late-type dwarfs, interacting binaries and a wide range of young stellar objects. Most of these object samples are inhomogeneous, and some contain very few identified members. This scarcity and heterogeneity places obstacles in the way of testing current models for the formation and evolution of these systems. Large-scale Hα surveys can be used to expand the known samples and to improve their homogeneity. Surveys of the highly populous Galactic Plane should be particularly successful in this regard.

Most previous photographic Hα surveys suffered from bright limiting magnitudes and/or small survey areas. Examples of such surveys include the Hα observations of the Large and Small Magellanic Clouds by Davies et al. (1976) and the Kyoto photographic survey of the northern Milky Way (University Kyoto 1982). Recent CCD imaging surveys such as the Virginia Tech H-alpha and [S II] Imaging Survey of the Northern Sky (Dennison et al. 1998, 1999) and the Southern Hα Sky Survey Atlas (Gaustad et al. 2001) cover large areas of the sky, but at relatively low spatial resolution. The Wisconsin Hα Mapper Northern Sky Survey (Haffner et al. 2003) has spectroscopically surveyed the Galaxy with a resolution of 1°. This has enabled the distribution and kinematics of diffuse H II to be mapped, but point source emitters could not be investigated.

This leaves an obvious gap for deep Galactic Hα surveys covering large areas at high spatial resolution. This gap has been partially filled by the photographic AAO/UKST Hα Southern Galactic Plane Survey (Parker et al 2005), which covers the latitude range, $|b| \leqslant 10^{o}$, down to ∼19.5 mag at a spatial resolution of 1″-2″. The INT/WFC Photometric Hα Survey (IPHAS, Drew et al. 2005) is a highly analogous survey of the northern Galactic Plane, in terms of both depth and spatial resolution. Now close to completion, its coverage in broadband r', i' and narrowband Hα is limited to the Galactic latitude range $|b| \leqslant 5°$. It differs also in being digital, allowing greatly superior photometric calibration, and the opportunity to photometrically select emission line stars across the northern Plane with high confidence. Here we present the first catalogue of IPHAS emission line stars, timed to accompany the first major release to the world community of general IPHAS photometry (González-Solares et al. 2008, in preparation).

The most extensive previous catalogue of emission-line stars in the northern Galactic plane has been compiled by Kohoutek & Wehmeyer (1999, hereafter KW99). The KW99 catalogue contains 4174 objects within the latitude range $|b| \leqslant 10^{o}$. Eighty per cent of the objects fall in the latitude range $|b| \lesssim 5^{o}$. The catalogue is expected to be complete to ∼ 13 mag, although 27 per cent of the objects are fainter than this, and 13 per cent do not have a measured brightness. Down to ∼ 13th magnitude, early-type emission line stars dominate the lists compiled by KW99, accounting for around three-quarters of all objects listed.

The catalogue presented here covers the magnitude range $13 \leqslant r' \leqslant 19.5$ mag. It is easily cross-matched to source lists in other wavebands and is already providing the basis for a range of spectroscopic follow-up programmes. In Section 2, we briefly describe the IPHAS photometric observing strategy. Section 3 discusses the selection algorithm used to construct our catalogue. Section 4 provides an overview of the catalogue and of the spatial distribution of the catalogue objects. In Section 5, we analyze the magnitude and colour distributions of our Hα-excess sources. Section 6 discusses the relative contributions of different stellar types to the catalogue, based on matches to the KW99 catalogue and to SIMBAD objects, and comments on preliminary results from our own spectroscopic follow-up observations. In Section 7, we summarize our main results and conclusions.

2 OBSERVATIONS

The data used to construct our point-source Hα-excess catalogue are composed of the IPHAS Galactic plane observations obtained between September 2003 and January 2007. After rejecting observations failing the IPHAS data quality criteria (see Section 3.1), these data cover about 80 per cent of the final survey area. Once the survey has been completed, we will update the online version of the catalogue to cover the final area.

Full details of the IPHAS observing strategy, data reduction, calibration and matched catalogue generation may be found in Drew et al. (2005); Irwin & Lewis (2001) and Irwin (1985). Briefly, all observations were obtained using the Wide Field Camera (WFC) on the Isaac Newton Telescope (INT), which gives a spatial pixel size of 0.33″x 0.33″ over a field of view of approximately 0.3 square degrees. Photometry was carried out using a set of three filters, comprising a narrowband Hα filter and the broadband Sloan r' and i' filters. Exposure times were 120 s for the Hα images, 10 s for the i' band images, and 30 s [10 s] seconds for all r' band images obtained after [before] June 2004.

Note that in all of our analysis below, we only work with sources brighter than $r' = 19.5$. In principle, IPHAS goes deeper than this, as the average r' band 3σ magnitude limit in the IPHAS fields used to construct the catalogue is $' = 21 \pm 1$. However, the increased photometric scatter and incompleteness at the faintest magnitudes makes it counterproductive to push our Hα-excess selection to this depth. We also adopt a bright limit of $r' = 13$ to exclude saturated objects.

The tiling pattern of the IPHAS survey is designed to ensure that objects are not routinely lost in the chip gaps of the INT/WFC CCDs. This is achieved by taking two observations for each pointing; here, we refer to these as the direct field and the offset field. The offset fields are located 5 arcmin W and 5 arcmin S of the direct field centres, and are identified by the letter "o" following the numerical field code. The existence of the offset fields means that the vast majority of objects in the survey (∼ 95%) are observed at least twice. As explained further below, we exploit this to improve the robustness of our Hα-excess selection.

3 SELECTION STRATEGY

3.1 Data Quality Constraints

Only data from fields that pass strict quality acceptance criteria were used to construct our catalogue. The two most important criteria are:

(i) the seeing in each band must not be greater than 2 arcsec;
(ii) the average stellar ellipticity in the images of each band must not be greater than 0.2.

This leaves 12959 IPHAS fields, providing an effective sky coverage of $\sim 1500\,\mathrm{deg}^2$. We also apply additional quality cuts at the level of individual sources. Thus each object in our catalogue

(i) must be detected at least twice in the survey (usually in a direct field and its offset field);
(ii) must be selected as an Hα-excess source in *both* detections (see Section 3.2 for details on the selection algorithm);
(iii) must have an r' magnitude in the range $13 < r' < 19.5$;
(iv) must not be flagged as severely blended;
(v) must be classified as stellar in the i' band, and stellar or probably stellar in the r' and Hα bands.

Cut (v) is imposed because our catalogue is intended mainly as a list of *stellar* emission line sources. Objects classified as probably stellar in the r' and Hα bands are nevertheless included to allow for compact nebulae and emission line stars with marginally resolved Hα shells (such as novae).

As a final precaution, we assign a flag 'c' to all objects in our catalogue for which the two r' measurements, the two $r'-i'$ colours or the two r'-Hα colours disagree by more than 0.3 mag. This could signal genuine variability, but can also occur if the photometric calibration of one field is incorrect due to partial cloud cover (a few such fields may be expected to survive all our quality cuts). Our selection algorithm is actually fairly insensitive to photometric zero-point offsets, but the photometry of emitters with inconsistent magnitudes/colours should be regarded with caution. All of the analysis in this paper is restricted to stars and emitters whose magnitudes and colours agree to better than 0.3 mag, unless explicitly stated otherwise in the relevant figure captions.

Only one set of photometric data is listed for each object in the catalogue, as derived from the highest quality field in which the object was detected. Throughout this paper, we will use the term field to refer to a single direct or offset field, and pointing to refer to them jointly (e.g. an object detected in a pointing is detected in *both* a field and its offset field).

3.2 Selecting Hα Emitters

Hα-excess sources are selected from the 12959 IPHAS fields using the algorithm described in Witham et al. (2006). The selection process is illustrated in Fig. 1. Briefly, we generate $(r'-i')$ versus $(r'-\mathrm{H}\alpha)$ colour-colour plots for each magnitude bin in each field. We then carry out an initial straight-line least-squares fit to all objects in each magnitude bin. However, many IPHAS fields exhibit (at least) two separate stellar loci in the colour-colour plane, due to differential reddening and/or contributions from both main-sequence stars and giants. We therefore use an iterative σ-clipping technique to force the fit onto the uppermost locus of points in the colour-colour diagram; this upper locus generally represents the unreddened main sequence. In cases where the final fit is poorer than the initial fit (e.g. in fields containing only a single stellar locus), we revert back to the initial fit. Once the appropriate fit for each magnitude bin has been found, we identify objects significantly above the fit as likely Hα emitters. In doing so, we take into account both the scatter of points in the stellar loci and the errors on the colours of each individual datapoint.

As explained in Witham et al. (2006), this automated selection process works well most of the time, but it can occasionally fail. The usual cause is a failure of the algorithm to satisfactorily identify the true upper edge of the stellar locus in the colour-colour diagram. In the present context, the most serious problem arising from this is that several of the objects belonging to this locus may be selected erroneously as Hα-excess sources. In the worst of these cases, the number of objects selected from a field will be abnormally high.

In practice, we find that the probability of algorithm failure becomes significant for fields where 10 or more objects were selected automatically. We therefore visually inspect the colour-colour plots for all such fields and replace the automated selections with manually identified ones. In doing so, we also keep track of fields where the colour-colour plots look genuinely unusual, so that it is hard to identify true emitters with confidence; objects selected from such fields are flagged in the catalogue. In total, 328 fields have been manually inspected, and 231 of the objects selected by the automated algorithm in these fields have been culled. However, the final catalogue still contains 752 manually-selected objects from these fields.

In spite of all the data quality controls we impose and the care we have taken to design a robust selection procedure, it is, of course, impossible to guarantee that every object in our catalogue is a definite Hα emitter. However, as discussed in Section 6.1.3, spectroscopic follow-up observations of ~ 300 objects from our catalogue with $r' \leqslant 18$ have confirmed the presence of Hα emission in about 97 per cent of this sample.

It is much harder to establish the completeness of our selection procedure, i.e. the fraction of Hα emitters selected as a function of magnitude, broad-band colour and equivalent width. Qualitatively, it is clear that the minimum equivalent width (EW) above which an object will be selected increases with increasing magnitude and reddening (see Fig. 1 and discussion in Drew et al. (2005)). However, the only way to determine the completeness quantitatively is to obtain spectra for a large, representative sample of objects (not just likely emitters). Such a large-scale completeness analysis has not yet been carried out. The more limited follow-up observations we have analyzed so far indicate that, as expected, our selection method is robust and conservative, rather than highly complete.

4 RESULTS

The full catalogue of Hα emitters is only available in electronic form and can be obtained at http://www.iphas.org or via VizieR at http://vizier.u-strasbg.fr/viz-bin/VizieR. As noted in Section 2, it currently covers 80% of the final IPHAS survey area, but will be updated once the survey has been completed. The first few entries in the catalogue are given in Table 1.

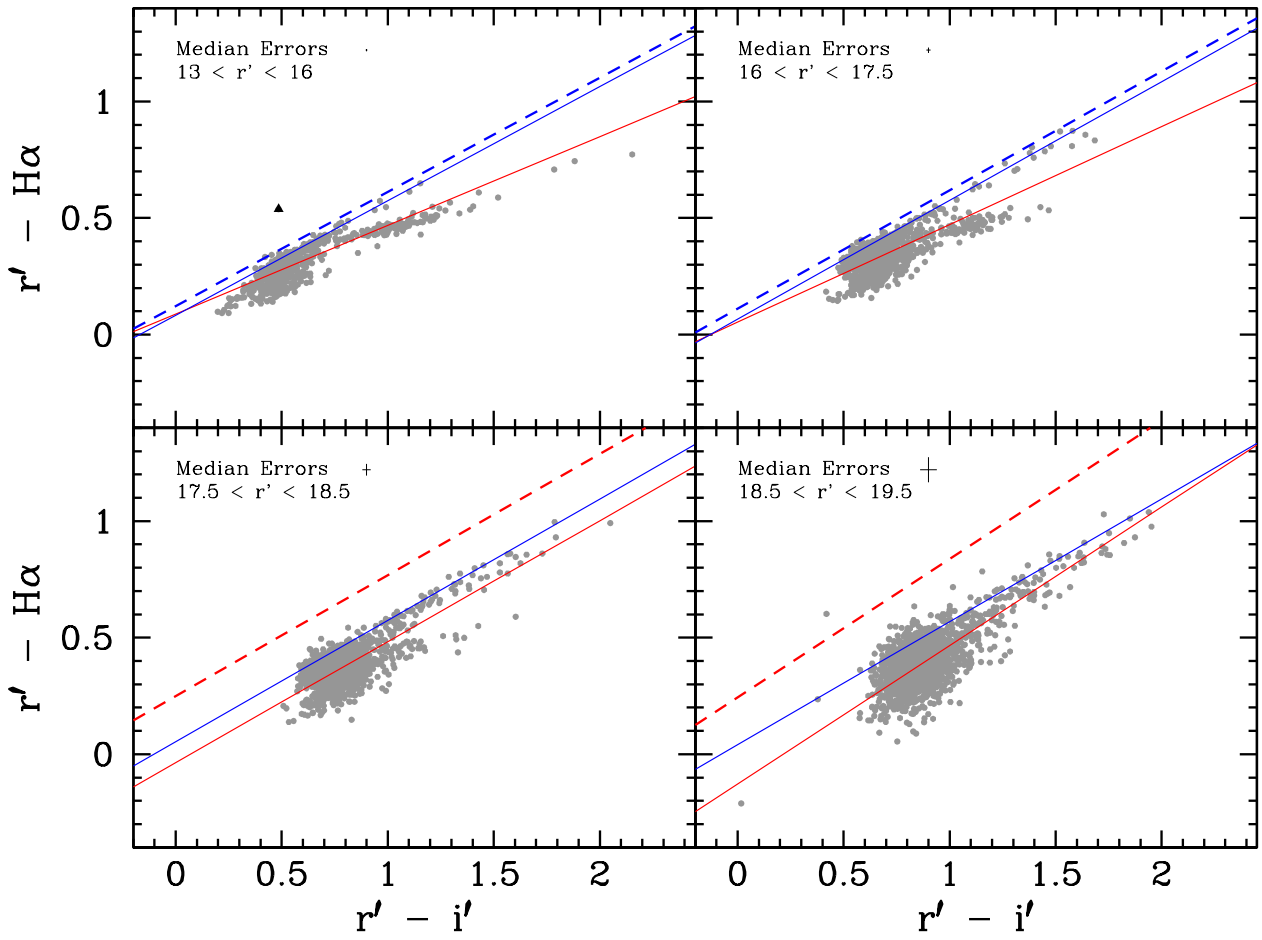

Figure 1. An illustration of the selection criteria used to identify strong emission line objects via colour-colour plots. The data shown here are all from the IPHAS field 2373. The data are split up into four magnitude bins, as shown in the four panels. The median errors of the datapoints in each bin are shown by the black crosses near the top of each plot. Objects with Hα excess should be located near the top of the colour-colour plots. The thin red lines illustrate the original least squares fit to all the data (grey points). The thin blue lines represent the final fits to the upper locus of points obtained by applying an iterative σ-clipping technique to the initial fit. The actual cuts used to select Hα emitters are shown by the thick dashed lines. If the cut was based on the initial [final] fit, it is shown in red [blue]. Objects selected as Hα emitters must be located above the cut and are shown as large triangles. Note that the cut lines shown here are only approximate, as the actual selection criterion also considers the errors on each individual datapoint. This explains, for example, why an object in the bottom right panel is not selected despite clearly lying above the cut line.

4.1 Basic Number Statistics

Our Hα-excess catalogue contains 4853 objects selected from 12959 fields. This represents an order of magnitude improvement in the number of faint ($r' \geqslant 13$) Hα emitters in the Northern Galactic Plane (Section 6.1). The final catalogue constructed from the completed IPHAS survey should therefore contain at least 6000 objects, even without any improvements to the selection technique. It is nevertheless worth working towards such improvements: extrapolation of the KW99 and Stephenson & Sanduleak (1971) surveys suggest that 10,000 - 40,000 objects could be uncovered by IPHAS if a more relaxed (or simply better) selection technique could be used.

The number of objects in our catalogue corresponds to an average surface density of ~ 3 Hα emitters per square degree in the Northern Galactic Plane. Similarly, we find that roughly 1 in 7000 stars are selected as Hα emitters. The conservative nature of our selection technique means that these numbers should be viewed as lower limits.

4.2 The Spatial Distribution of Hα Emitters

4.2.1 The 2-D Distribution of Hα Emitters

Fig. 2 shows the 2-D distribution of all catalogue objects in Galactic latitude and longitude, along with the distribution of all parent fields from which the catalogue was created. On average, the surface density of Hα-excess objects is highest near the Galactic Equator, particularly in the longitude range 60–140°. This reflects the increasing density of Hα emitters near the mid-plane of the Galactic disc. The surface density of emitters is also rather non-uniform (cf KW99).

Table 1. IPHAS positions, magnitudes and colours of the first few objects in the catalogue of point-source Hα emitters. The full catalogue is available from http://www.iphas.org or from VizieR

IPHAS name/position J[RA(2000)+Dec(2000)]	**IPHAS photometry** r'	$r'-i'$	$r'-$Hα	**flag**[a]	**SIMBAD match flag**[b]
J000000.18+645440.7	17.231 ± 0.005	0.861 ± 0.009	0.680 ± 0.009		
J000039.05+623316.6	14.168 ± 0.002	0.217 ± 0.003	0.271 ± 0.003	c	
J000137.14+620423.4	16.944 ± 0.005	0.410 ± 0.011	0.361 ± 0.010		
J000213.37+645424.6	16.969 ± 0.010	0.856 ± 0.013	1.346 ± 0.011	ck	C/Em*=RI* (*,V*)
J000220.16+594538.7	14.447 ± 0.001	0.439 ± 0.002	0.427 ± 0.002		
J000250.83+634633.7	15.388 ± 0.002	0.760 ± 0.004	0.651 ± 0.004		
J000259.61+620916.3	14.983 ± 0.002	0.723 ± 0.004	0.794 ± 0.004		
J000301.71+621020.3	14.276 ± 0.001	0.725 ± 0.002	0.764 ± 0.002	k	UC/Em*
J000315.54+625423.0	15.257 ± 0.002	0.519 ± 0.004	0.475 ± 0.004		
J000335.07+632946.2	13.792 ± 0.002	0.566 ± 0.003	0.675 ± 0.002	k	UC/Em*
...					

[a] This column is used to flag any special circumstances related to the photometry or if the object is in the vicinity of a KW99 object. Possible entries in this column are as follows: c - the object does not have consistent magnitudes in any of the IPHAS fields used to construct the catalogue. This can be as a result of source variability or poor photometric calibration as a result of observing in less than ideal conditions. m - the object is located in a field where manual selection of emitters took place. o - the object is located in a field where manual selection of emitters took place and additionally the distribution of objects in the colour-colour plots from this field looked unusual. k - the object has been matched with a previously known Hα emitter in KW99 with a matching radius of up to 30 arcsec.

[b] An entry in this column indicates that the object is matched with a SIMBAD object. Entries begin with either UC/ or C/ followed by the short-hand main SIMBAD classification. UC/ designates objects whose main object type falls within the 8 broad classifications defined in Section 6.1.2. The maximum matching radius for these objects is listed in Table 2. C/ designates those objects whose main object type is not one of the 8 main types. These objects have a generally finer classification and have a maximum matching radius of 10 arcsec. For the C/ objects the other possible object types listed in Simbad are also given in parenthesis. The C/Em* entries are the SIMBAD objects whose main object type is not Em* but have Em* listed as another object type. If these objects are within 10 arcsec of the IPHAS source then the object is designated by C/Em*= followed by the main object type. If the object is located at a distance greater than 10 arcsec (but still within the 45 arcsec matching radius used for objects whose main type is Em*), then the object is designated by C/Em* ∼ followed by the main object type.

This is to be expected, since the density of Hα emitters will be enhanced near clusters, OB associations, etc.

We have visually identified some of the most prominent overdensities in Fig. 2, concentrating especially on areas rich in faint emitters. These regions are as follows:

(i) $l \sim 60$, $b \sim 0$: This region coincides with the OB association Vul OB1 and, on smaller scales, the central cluster of this association. This cluster, NGC 6823, is already known to harbour at least 2 Be stars (Shi & Hu 1999).

(ii) $l \sim 68$, $b \sim 1$: This overdensity of mainly bright emitters is close to the HII region Sharpless 2-98, which is ionized by the Wolf-Rayet star W130 (Cichowolski et al. 2001). The WR star itself is in the KW99 catalogue, as are several other objects in the vicinity of this star-forming complex.

(iii) $l \sim 99.5$, $b \sim 3.5$: This overdensity is coincident with the young open cluster Trumpler 37, which belongs to the Cep OB2 (Marschall et al. 1990). Several Hα emitters have already been found in this region (e.g. Kun & Pasztor 1990).

(iv) $l \sim 105$, $b \sim 4.0$: This overdensity appears to be connected to the LDN 1188 dark cloud complex. This may in turn belong to the Cepheus bubble and is known to contain several T Tauri stars and other Hα emitters (Abraham et al. 1995). Drew et al. (2005) present multi-object spectroscopy entered on $l \sim 105.6$, $b \sim 4.0$ and find 29 definite Hα emitters in the magnitude range $17 \leqslant r' \leqslant 20.5$.

(v) $l \sim 110.5$, $b \sim 3.0$: This area lies within the Cep OB3 association which contains many previously known Hα emitters (see, for example, Mikami & Ogura 2001).

(vi) $l \sim 135$, $b \sim 1.5$: This location lies close to several BRCs that are known to harbour Hα emitters. Two examples are BRC 5 and 7 (Ogura et al. 2002). The OB association Cas OB6 also lies nearby. The central cluster of this association, IC 1805, is known to contain early-type emission-line stars Shi & Hu (1999).

(vii) $l \sim 138$, $b \sim 1.5$: This region coincides with bright rim cloud (BRC) 14, which is already known to harbour 47 Hα emitters (Ogura et al. 2002).

(viii) $l \sim 173$, $b \sim -0.25$: The OB association Aur OB2 is located in this region of the sky, along with the H II region IC 417. However, we have not been able to identify clusters, BRCs or other object of smaller spatial scale near this location.

Other spatial features traced by the catalogue of Hα emitters can be more readily identified by collapsing the information in Fig. 2 to one dimension. The histograms in Fig. 3 and Fig. 4 show the distribution of objects in Galactic longitude and latitude. What is actually plotted in these figures is the number of Hα emitters per longitude/latitude bin, divided by the number of IPHAS pointings in that bin. This normalization helps to remove the effects of spatial variations in survey coverage.

4.2.2 The Longitude Distribution of Hα Emitters

The top panel of Fig. 3 shows the distribution of catalogue objects in Galactic longitude. This distribution shows a multitude of peaks and troughs over the region surveyed. OB associations, clusters, bright rimmed clouds, and other re-

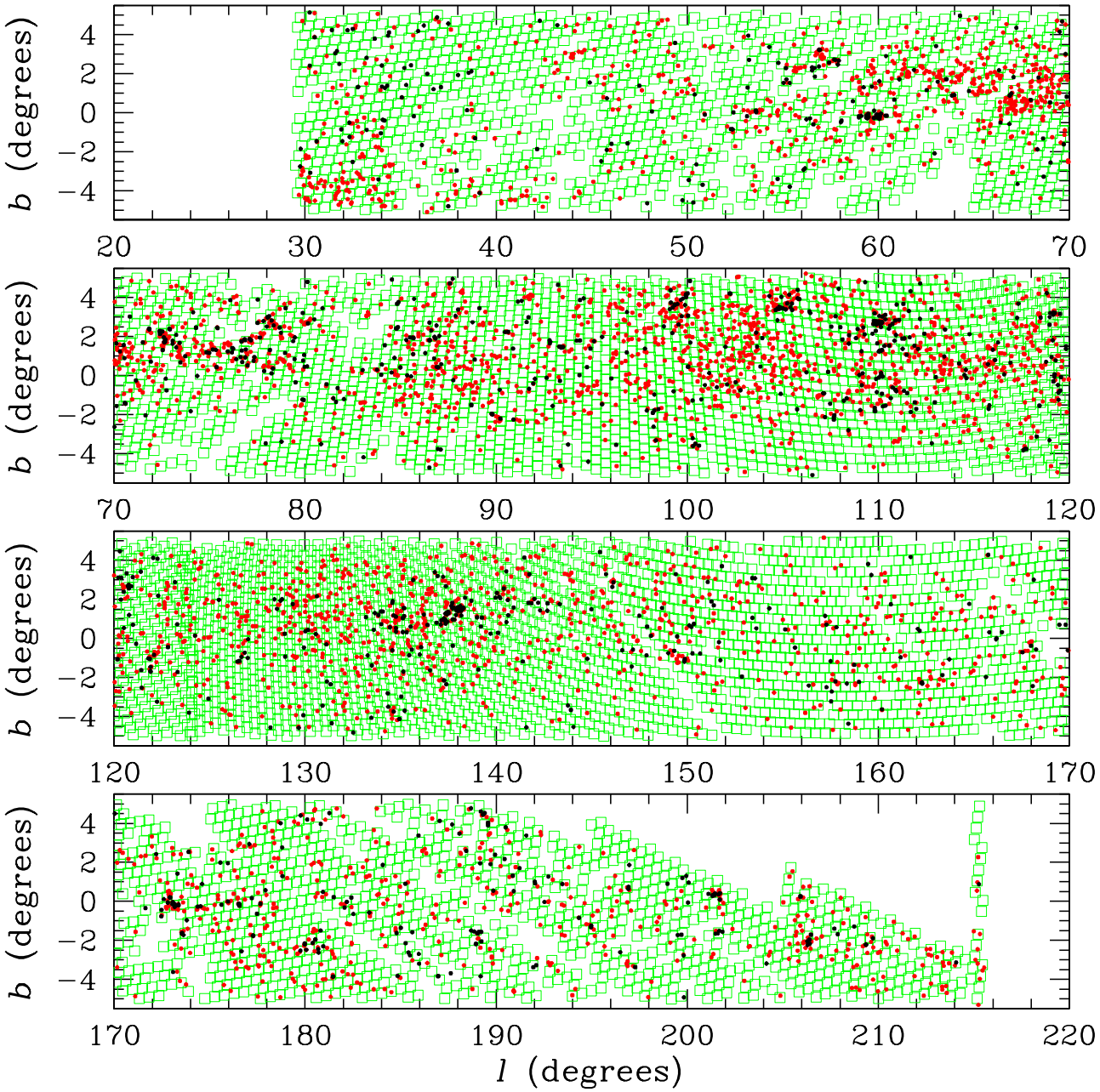

Figure 2. The distribution of Hα emitters in Galactic longitude and latitude. The emitters are shown as red points if brighter than $r' = 18$, and black points if fainter. The IPHAS direct fields are shown by green squares (offset fields are not shown). All emitters are shown here, including those with flagged with 'c' in Table 1.

gions of active star formation can cause local peaks in the distribution. Several of the most prominent peaks have been labelled with the names of the objects that are likely responsible for these overdensities.

The middle panel shows the distribution of all stars, again divided by the number of catalogue pointings in each spatial bin. The green and grey vertical lines at $\ell = 33^{\rm o}$ and $\ell = 55^{\rm o}$ in this panel mark the locations of the tangent directions reported by Bronfman (1992), that are now seen as associated with the Scutum-Crux and Sagittarius-Carina arms (see e.g. Russeil 2003). In the top panel of Fig. 3, there is evidence of a peak in the range $30^{\rm o} < \ell < 35^{\rm o}$ in the surface density of Hα emitters (see also Fig. 2). The all-star sample also peaks here, and so both emission line and normal stars appear to be somewhat more abundant in the vicinity of the first tangent point.

In between the $\ell = 33^{\rm o}$ and $\ell = 55^{\rm o}$ tangents, there are relatively few candidate emission line stars, even though the surface density of normal stars climbs. This is where the Sagittarius-Carina arm might be expected to be most prominent. The scarcity of emission line stars in this region may be due to a combination of high reddening and limited

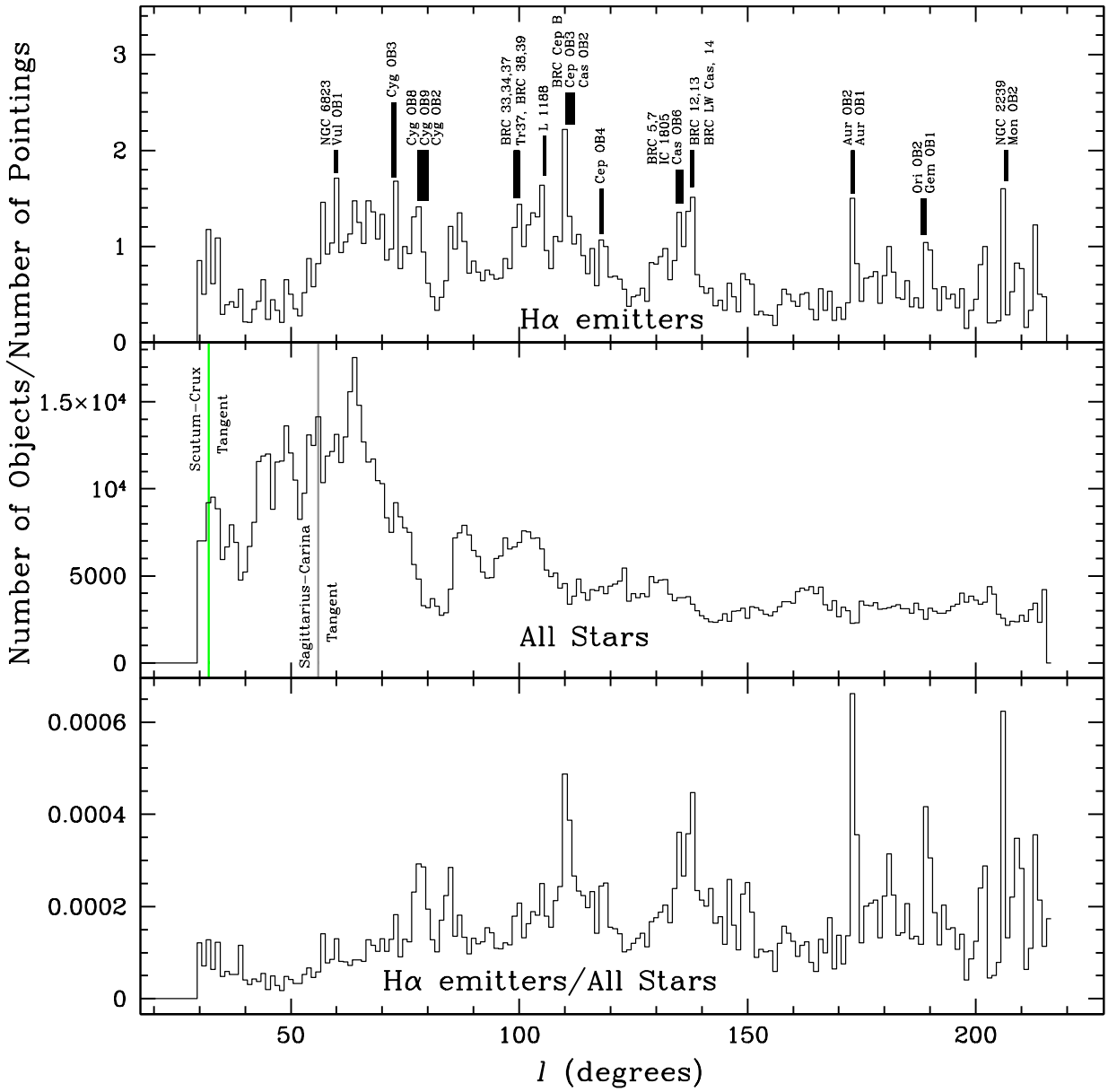

Figure 3. The distribution of Hα emitters in Galactic longitude. The top panel shows the distribution of Hα emitters divided by the number of pointings in each spatial bin. OB associations, BRCs, and clusters whose position coincide with peaks in the distribution are labelled. The width of the lines marking the peaks illustrates the spread in the central locations of the different regions that are appropriate to that peak. The middle panel shows the distribution of all stars divided by the number of pointings in each spatial bin. The bottom panel shows the ratio of the two distributions. The bin width for all the distributions is 1°. The green and grey vertical lines in the middle panel show the location of the tangents to the Scutum-Crux and Sagittarius-Carina arms respectively (Bronfman 1992, Russeil 2003).

Hα emission equivalent width (under 30 to 40 Å, figure 6 in Drew et al. 2005). The highly extincted Aquila Rift lies within this region, for example. Weak emission line stars within or beyond such local absorbing structures could be well concealed. This will warrant further investigation.

At longitudes beyond $\sim 60^{\rm o}$, the surface densities of both emission line stars and normal stars show a general decline, interrupted by much finer scale structure. Over this range, out to $\ell \simeq 215^{\rm o}$, the major Galactic structures are expected to be the Perseus arm and the rather more uncertain Outer, or Norma-Cygnus, arm. The most prominent localised feature in the all-star sample distribution is the broad and deep dip at $\ell \sim 80^{\rm o}$ linked with the highly obscured Cygnus-X region. This drop is less marked in the

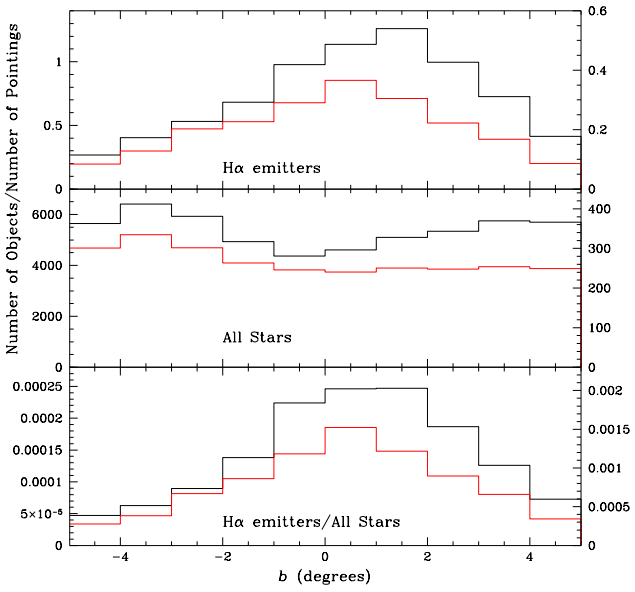

Figure 4. The distribution of Hα emitters in Galactic latitude. The black histograms (corresponding to the left vertical scales) show the distributions of objects irrespective of r' band magnitude. The red histograms (corresponding to the right vertical scales) show the distribution of the bright objects only ($r' \leqslant 15$). The top panels show the distributions of Hα emitters (divided by the number of pointings in each spatial bin). The middle panels show the corresponding distributions of all stars. The bottom panels show the ratios of emitter and all-star distributions.

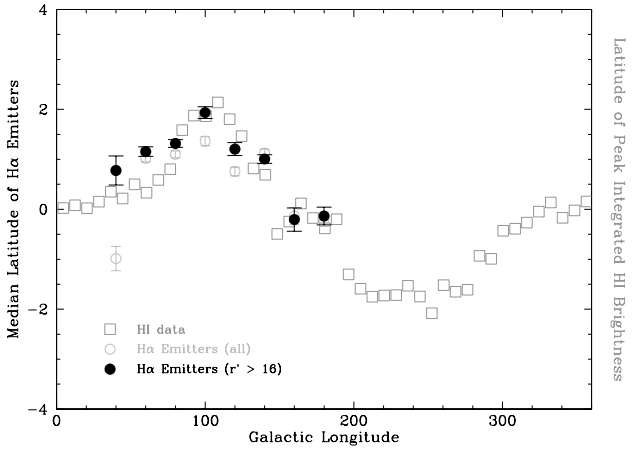

Figure 5. The median latitude as a function of longitude for all Hα emitters (open circles) and faint Hα emitters (($r' > 16$; solid circles), compared to the peak latitude of integrated H I brightness (open squares; measured from Fig. 3 in Freudenreich et al. 1994). The signature of the Galactic warp is obvious in the H I data, and probably also be present in the Hα data.

Hα emitter distribution, and hence appears as a relative (if doubled) peak in the ratio distribution. Cygnus X is known to harbour much star formation (e.g. Odenwald & Schwartz 1993).

4.2.3 The Latitude Distribution of Hα Emitters

The top panel of Fig. 4 shows the distribution of catalogue objects in Galactic latitude. The black histogram reveals that the density of Hα-excess objects actually peaks at latitudes between 1° and 2°. This contrasts with the result from KW99, who find that the distribution of bright Hα emitters peaks close to the Galactic Equator. The difference is mainly due to the inclusion of fainter Hα emitters in the IPHAS catalogue. When we consider only objects with $r' \leqslant 15$ (red histograms in Fig. 4), we find a similar latitude distribution to KW99. The central dip in the latitude distribution of the all-star samples is due to the high extinction near the Galactic equator.

The latitude distribution of Hα emitters is also longitude dependent. This is illustrated in Fig. 5, which shows the median latitude of our Hα emitters as measured in 20° longitude bins. These data can be compared directly to the latitude of peak integrated H I brightness of the Galactic disk (open squares in Fig. 5; taken from Freudenreich et al. 1994). The H I data clearly show the signature of the Galactic warp. The strong similarity between the H I peak brightness and the median Hα emitter latitude seen in Fig. 5 suggests the latter may also trace the warp. This is quite reasonable, given that our catalogue is probably dominated by young objects (and particularly early-type stars; see Sections 5.4 and 6.1.3). Both the integrated infra-red light of the stellar Galactic disk (Freudenreich et al. 1994), as well as OB stars specifically (Miyamoto et al. 1991), are already known to trace the warp.

Fig. 5 also suggests that the probable warp signature is somewhat clearer if only fainter emitters ($r' > 16$) are considered. This, too, is plausible. As shown in Marshall et al. (2006), the warp is more prominent at larger distances from the Sun (beyond a few kpc), plus heavy *local* extinction may prevent any such signature showing in the bright emitter population at some longitudes – particularly those well inside the Solar Circle ($\ell \lesssim 60°$). For example, the heavy local ($\lesssim 2$ kpc) extinction associated with the Aquila Rift may be responsible for the deficit of bright emitters at positive latitudes around $\ell \simeq 30°$ (cf. Figures 7 and 8 in Marshall et al. 2006).

5 THE PHOTOMETRIC PROPERTIES OF Hα EMITTERS

5.1 The $(r' - H\alpha)$ vs $(r' - i')$ Distribution of Hα Emitters

Fig. 6 shows the distribution of catalogue objects in the $(r' - H\alpha)$ vs $(r' - i')$ colour-colour plane. This is the plane used by our selection algorithm (cf Fig. 1). We recall that our algorithm works by identifying objects located above the upper stellar locus in each field, and that this locus is usually composed of unreddened main-sequence stars (Section 3.2). In line with this, Fig. 6 shows that the vast majority of our Hα-excess sources lie above the expected location of the unreddened main sequence. The few objects below this line may still be genuine emitters (e.g. they could come from fields in which the absolute photometry is somewhat compromised), but their status is less certain.

Following Witham et al. (2006) and Drew et al. (2005),

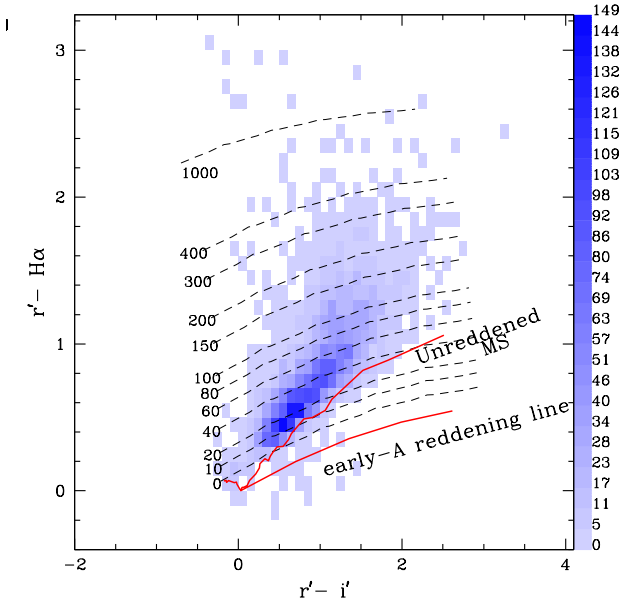

Figure 6. The distribution of Hα emitters in the $(r'-\mathrm{H}\alpha)$ versus $(r'-i')$ plane. The shade of blue assigned to each grid square in the colour-colour plane indicates the number of emitters it contains, as defined by the contrast scale on the right. The expected locations of the unreddened main sequence and the early-A star reddening line are also shown. The dashed lines represent lines of constant Hα equivalent width (in Å as labelled) for early-type stars. These lines move from left to right with increasing reddening. All emitters are counted here, including those flagged with 'c' in Table 1.

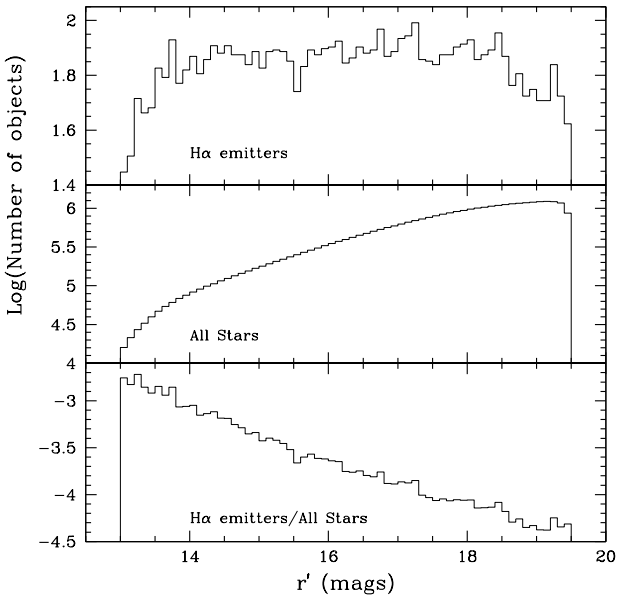

Figure 7. The r' band magnitude distribution of Hα emitters in the catalogue along with the distribution of the all-star sample and the ratio of the two.

we have also indicated in Fig. 6 lines of constant Hα EW for stars with relatively blue spectral energy distributions (see Drew et al. 2005 for details). This shows that a reddened early-type emission line star must have considerably higher EW to make our selection cut than an unreddened one.

5.2 The Magnitude Distribution of Hα Emitters

In the top panel of Fig. 7, we show the r' magnitude distribution of our catalogue objects. The fact that this distribution is flat in the range $14 \lesssim r' \lesssim 18$ is not an indication of completeness. After all, as shown in the middle panel of Fig. 7, the total number of stars (not just emitters) rises steeply towards fainter magnitudes almost all the way to the catalogue limit. Thus the fraction of objects selected as Hα emitters is a strongly decreasing function of magnitude (bottom panel of Fig. 7). This mainly reflects the fact that it is much easier to select bright Hα emitters than faint ones.

This statement can be quantified. The minimum Hα EWs for inclusion in the catalogue can be estimated from the IPHAS photometry using the techniques described in Witham et al. (2006) and Drew et al. (2005); see also Fig. 6). In principle, this limiting EW depends on both the intrinsic SED shape and the observed broad-band colour. Here, we simply adopt $(r'-i') \simeq 1$ as representative for our catalogue objects and take their SEDs to be reddened Rayleigh-Jeans spectra (many of them will be early-type emission line stars; see Section 6.1.3). *For these choices of SED and colour*, we then estimate limiting EWs of ~ 15Å in the range $r' = 13-17.5$, ~ 25Å in the range $r' = 17.5-18.5$, and ~ 50Å in the $r' = 18.5-19.5$.

5.3 The $r'-\mathrm{H}\alpha$ Distribution of Hα Emitters

Fig. 8 shows the $(r'-\mathrm{H}\alpha)$ distribution of catalogue objects, separated into two coarse magnitude bins. The emission line star populations produce a distinct "shoulder" in the $(r'-\mathrm{H}\alpha)$ distributions of the all-star samples. The fraction of stars selected as emitter rises monotonically with Hα excess, until at sufficiently large excesses, almost all objects are selected. For bright stars, this happens beyond $(r'-\mathrm{H}\alpha) \simeq 1.6$; for faint stars, it only happens beyond $(r'-\mathrm{H}\alpha) \simeq 2.3$. More generally, at any given Hα excess, the fraction of objects selected is larger for bright objects than for faint ones. The peak in the number distribution of bright emitters also lies at substantially smaller $(r'-\mathrm{H}\alpha)$ values.

All of these results are in line with expectations: once the Hα-excess of emission line objects becomes significantly larger than the dispersion of ordinary stars in $(r'-\mathrm{H}\alpha)$, the probability that they will be selected rises monotonically with increasing excess. At any given Hα excess, this probability is higher for bright objects, since the dispersion caused by photometric scatter is smaller for them. On the other hand, the *intrinsic* Hα-excess distribution of Galactic emission line stars is likely to rise monotonically towards smaller excesses (i.e. there are more weak line emitters than strong ones). The location of the peaks in the observed $(r'-\mathrm{H}\alpha)$ distributions of emitters is thus set by the competition between these effects.

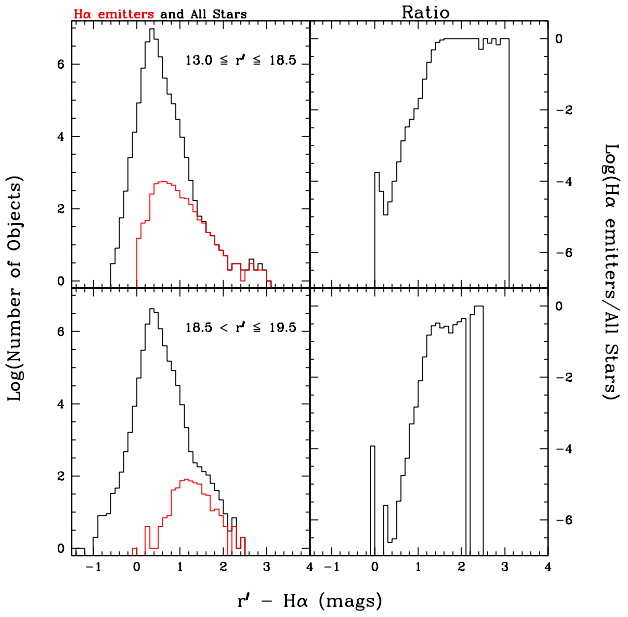

Figure 8. The $(r' - \mathrm{H}\alpha)$ distribution of Hα emitters in the catalogue along with the distribution of the all-star sample and the ratio of the two. The left hand panels show the distribution of the Hα emitters (red histograms), overplotted on top of the distribution of the corresponding all-star samples (black histograms). The right hand panels show the ratio of the emitter and all-star distributions. The top panels show the distributions of bright objects ($r' \leqslant 18.5$; the bottom panels show the distributions for fainter objects.

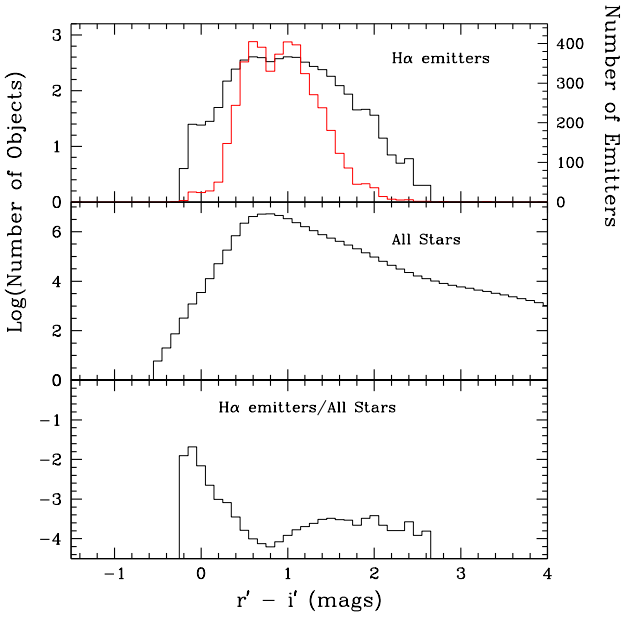

Figure 9. The $(r' - i')$ distribution of Hα emitters along with the distribution of the all-star sample and the ratio of the two. The black distributions are shown on a logarithmic scale (left axes); the red distribution in the top panel shows the emitter distribution on a linear scale (right axis).

5.4 The $r' - i'$ Distribution of Hα Emitters

Fig. 9 shows the $(r' - i')$ distribution of Hα emitters. The top panel shows the distribution of the catalogue objects themselves, the middle panel shows the distribution of the all-star sample, and the bottom panel shows the ratio of the two distributions.

The emitter distributions are clearly bimodal, as is particularly obvious for their fractional incidence relative to other stars. The blue peak is almost certainly dominated by early-type emission line stars (see Section 6.1.3). The existence of the red peak may reflect an increasing contribution of other objects, such as young/active late-type stars to the emitter population. However, spectroscopic follow-up of a significant sample of faint, red catalogue objects will be required to determine the make-up of this population with confidence.

6 DISCUSSION

6.1 The Nature of Hα-Excess Objects

One of the most important questions regarding our emitter catalogue concerns the nature and fractional contribution of different stellar populations to the overall sample. Below, we will attempt a preliminary answer to this question based on matches to existing star catalogues and initial spectroscopic follow-up observations of our own.

6.1.1 *Matches with the KW99 Catalogue*

Twenty-seven percent of KW99 objects are fainter than 13th mag, and we expect a significant fraction of these to be present in our catalogue also. We have therefore performed a positional cross-match between objects in the two catalogues. Magnitude information was not considered when matching, and only those 3543 objects in KW99 that fall inside the area covered by our catalogue were used.

In order to select an appropriate matching radius, and get a handle on the number of spurious matches, we created a mock catalogue in which all positions in the IPHAS Hα emitter catalogue were shifted by 0.5° in Galactic latitude and longitude. We found that the matching radius that maximizes the difference between matches to the real data and matches to the mock catalogue is 7.4 arcmin. This is about 5 times the positional uncertainty suggested by KW99 for stars belonging to their lowest accuracy category. With this matching radius, 1056 IPHAS emitters are matched to KW99 objects, whereas 536 matches are found for the mock catalogue. We therefore expect that ~ 500 objects (~ 10 per cent of the IPHAS sample) are common to both catalogues. Since a 50 per cent false match probability is not very helpful when it comes to identifying specific objects in common, we only flag matches to KW99 in our catalogue if the coordinates agree to better than 30 arcsec. With this matching radius, we expect only about 3 false matches amongst the 252 flagged objects (which represent about 5 per cent of the IPHAS-based catalogue).

It is interesting to compare the expected number of objects common to both catalogues (~ 500) to the magnitude distributions of the two catalogues. These are shown in Fig. 10 in both differential (top panel) and cumulative form

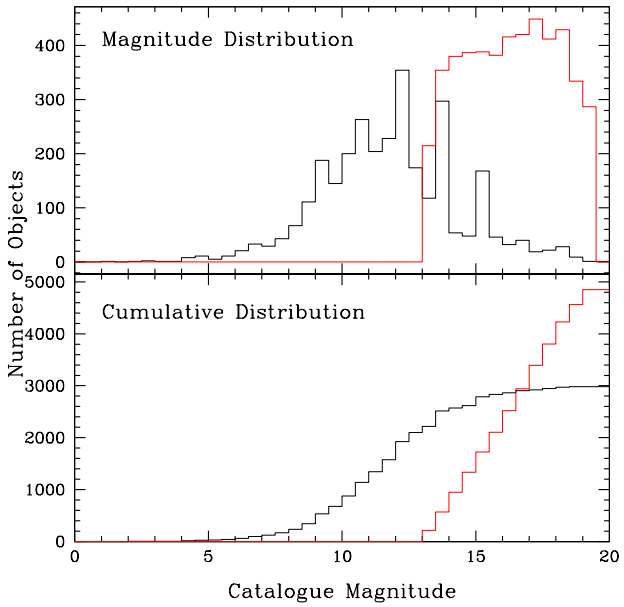

Figure 10. The magnitude distribution of the IPHAS catalogue of Hα emitters (red line) compared to the magnitude distribution of objects in the KW99 catalogue (black line). The IPHAS magnitudes shown correspond to the r' band, and the majority of the KW99 magnitudes correspond roughly to V band (based on either photoelectric, photographic or photovisual measurements). The top panel shows the magnitude distribution, and the bottom panel shows the cumulative distribution. All IPHAS emitters are shown here, including those flagged with 'c' in Table 1.

(bottom panel). In order to allow for a meaningful comparison, we have only considered the 2984 KW99 objects that fall inside the spatial area of the IPHAS catalogue and also have magnitude estimates. Ignoring the differences between the IPHAS and KW99 photometric band-passes for the moment, the magnitude distributions would suggest that ~ 900 objects should fall within the area and magnitude range covered by both catalogues. Allowing for the difficulty in comparing source magnitudes between the two catalogues, and the fact that ~ 400 of the overlapping objects in the KW99 magnitude distribution are located very close to the bright cut-off of the IPHAS catalogue, we suspect that this number is consistent with the approximate value derived from the positional cross-matches.

6.1.2 Matches with SIMBAD

We have also cross-matched the objects in our Hα-excess catalogue against previously known sources in SIMBAD. As a starting point, we initially searched for all objects in SIMBAD within 1 arcmin of the IPHAS positions. The results of this initial search showed that the majority of matches fall within 8 main categories. In order of most matches, these categories are: emission line stars (Em*), infrared sources (IR), normal stars (*), stars in clusters (*iC), stars in associations (*iA), radio sources (Rad), X-ray sources (X) and variable stars (V*).

As in Section 6.1.1, we used mock data sets to determine appropriate matching radii and estimate the number of spurious matches. In this case, the matching radius for each of the 8 main categories was chosen to keep the fraction of spurious matches below about 5 per cent. We allowed two exceptions to this rule: (i) the matching radius to X-ray sources was increased to allow an expected 10 per cent contamination fraction; (ii) the matching to IR sources was increased to allow an expected 8 per cent contamination fraction. In both cases, this was done because the total number of matches was still increasing significantly as a function of matching radius at the 5 per cent contamination level.

The resulting matching radii for each object class and the number of matches obtained are shown in the top part of Table 2. Within each object class, we have also looked for objects listed as emission line objects. This was done by checking the "other object type" field in SIMBAD.

As expected, the highest number of matches belong to the Em* category. The majority of these objects come from KW99, although there are a few additional objects from other sources. We have also included in Table 2 (in the row that is directly above the first set of totals) the number of matches to objects whose main object type is not Em*, but which have Em* defined as a secondary object type in SIMBAD. These are labelled as Em*2, and the matching radius used for these objects was the same as the Em* objects. A total of 316 IPHAS emitters have been matched with Em*/Em*2 in SIMBAD. This 7 per cent matching fraction is broadly consistent with the results of the previous section (a 5-10 per cent matching fraction depending on matching radius). Thus in the interval between the publication of KW99 and the present catalogue, only a small number of additional emitters appear to have been found in the Northern Milky Way.

Perhaps the most interesting matches are those to Infra-Red (IR), X-ray and Radio sources. The majority of the IR sources are IRAS identifications. These sources are often young stars still shrouded in dust, and the sources matched with IPHAS Hα emitters are likely T Tauri or Herbig-type objects. The 20 arcsec matching radius used for the IR sources is comparable to the positional uncertainty of IRAS sources (typically between 2 and 16 arcsec, but up to 1 arcmin in extreme cases). The X-ray matches are all ROSAT sources, and the 20 arcsec matching radius used is similar to the typical positional uncertainties of ROSAT sources (Voges et al. 1999). Note that 14 of the 26 X-ray sources, the majority of the IR sources and all of the radio sources have no other object associations or source classifications in SIMBAD. These sources are excellent follow-up candidates. Indeed, one of the X-ray sources has already been identified as a new CV candidate (IPHAS J052832.69+283837.6; Witham et al, submitted to MNRAS).

There are also a significant number of matches to SIMBAD objects that do not belong to the 8 main object classes listed above. Due to the small number of matches for each of these object types, it has not been possible to establish the best matching radius for each type. We have therefore simply adopted a 10 arcsec matching radius and searched for any IPHAS objects matched with SIMBAD objects other than those in the classes above.

Since rather a lot of different object types have been uncovered by this exercise, we only present a concise summary in the bottom part of Table 2. Thus we have grouped the various SIMBAD types into a coarser classification scheme that

Table 2. A summary of the results obtained from a positional cross-match between the catalogue of IPHAS emitters and SIMBAD. SIMBAD categories of objects are listed in the first column. The main categories of SIMBAD objects are listed in the top part of the table. The objects not included in the 8 main object types are listed in bottom part of the table. The SIMBAD short-hand object classifications are given in the second column. The final column lists the SIMBAD matches which have emission-line star listed as either the main object type or secondary object type.

Main object categories	associated SIMBAD object types[a]	matching radius (arcsec)	# of IPHAS emitters with SIMBAD matches	# of SIMBAD objects matched to IPHAS emitters	# SIMBAD objects classed as emitters
Emission-line Star	EM*	45	288	360	360
Infra-Red source	IR	20	106	111	1
Star	*	3	22	22	0
Star in Cluster	*iC	5	21	22	0
Star in Association	*iA	3	15	16	0
Radio-source	Rad	15	7	9	0
X-ray source	X	20	26	26	0
Variable Star	V*	20	13	14	4
Emission-line Star[b]	Em*2	45	28	35	35
Totals			526	615	400
Additional Object Categories					
Nebulae	BNe, HH, HII, PN, PN?, RNe, Cld, EmO	10	21	24	4
Interacting Binaries	CV*, DQ*, DN*, Al*, No*, NL* Sy*, XB	10	33	34	5
Young Stars	Y*O, TT*, FU*, Or*	10	16	16	1
Other Variable Star	Pu*, RI*	10	5	5	2
Other Star	Be*, C*, *i*, WD*, WR*	10	10	11	3
Misc	Cl*, G, Mas, ?, UV	10	11	14	0
Totals			96	104	15

[a] See http://vizier.u-strasbg.fr/viz-bin/Otype?X for a description of the SIMBAD classification scheme.
[b] These emission-line stars are those objects whose main object type is not listed as emission-line star but have emission-line star listed as a secondary object type.

combines related classes under one heading. We find that interacting binaries are the dominant population amongst these other matches. This is not surprising given that the majority of these objects are known to be Hα emitters. Several nebulae are also detected, which reinforces the fact that the catalogue is not completely free of extended objects. There are also matches to young stars and variable stars, as well as to variety of miscellaneous objects, including white dwarfs, carbon stars, Wolf-Rayet stars, masers, etc.

We finally note that there are only 4 matches to objects labelled as Be stars in SIMBAD, even though our own follow-up suggests that many objects in our catalogue belong to this class (see Section 6.1.3 below). The explanation is probably that most of the bright Be stars are simply labelled as Em* in SIMBAD, whereas most of the faint objects remain to be identified.

In total, we have found SIMBAD matches to 519 IPHAS objects. (This is lower than the sum of the total values in Table 2, because some IPHAS sources are matched to multiple SIMBAD objects with different classification.) This total number of matches suggests that $\simeq 90$ per cent of the IPHAS emitters are previously unknown systems. Thus IPHAS is uncovering a large new population of Hα emission line stars.

6.1.3 Spectroscopic Follow-up

Given that only a small fraction of the catalogue consists of previously known objects, a large-scale spectroscopic follow-up effort is necessary to determine the true make-up of the catalogue. Such an effort is underway, using both long-slit and multi-fibre spectroscopy. Here, we merely note that a first analysis of spectra for ~ 300 catalogue objects brighter than $r' = 18$ confirms $\simeq 97$ per cent of them as Hα emitters, with ~ 85 per cent belonging to broad class of early-type emission line stars (Witham 2007). This dominance of early-type emitters is consistent with the results of KW99. Interacting binaries, late-type stars and young stellar objects make up smaller fractions of this sample.

However, it is important to keep in mind that this early spectroscopic sample is limited to bright emitters and, partly because of this, also biased towards blue objects (Witham 2007). Thus the make-up of the fainter and redder Hα-excess population still needs to be explored. Broadly speaking, we should still expect to find many early-type emission line stars as we push to fainter magnitudes, because both the closest and the more distant spiral arms are expected to harbour significant populations of these objects. However, at these

fainter magnitudes, we may also expect to find an increasing proportion of interacting binaries, late-type stars, and T Tauri stars in star-forming regions. The often close grouping of the faint emitters in the 2-D distribution of emitters in the Galactic Plane shown in Fig. 2 provides evidence for the increased presence of emitters in star forming regions and associations at faint magnitudes.

7 CONCLUSIONS

A catalogue of Hα emitters selected from existing IPHAS photometry has been presented and analysed. The catalogue contains 4853 objects in the magnitude range $13 \leqslant r' \leqslant 19.5$ selected from $\sim$ 150 million objects in total. The average surface density of these Hα-excess objects is ~ 3 emitters per square degree. The true surface density of Hα-excess objects in the Galactic Plane is expected to be higher than this, due to the bias in the selection technique against detecting reddened earlier-type and/or weak-lined emitters, especially in regions where the surface density of emitters is high. The present catalogue is compiled from $\simeq$ 80 per cent of the final IPHAS survey area, leading to an expected number of at least $\sim$ 6000 Hα emitters from IPHAS, even with the very conservative selection procedure adopted here. Preliminary spectroscopic follow-up observations suggest that, at least to $r' \simeq 18$, more than 95% of our catalogue objects are genuine Hα emitters.

The $(r'-i')$ distribution of Hα emitters is bimodal, with a minimum near the peak in the distribution of the all-star sample (non-emitters). The blue peak in the emitter distribution is dominated by early-type emission line stars. The red peak is probably due to an increasing contribution of other types, most notably young/active late-type stars. The spatial distribution of catalogue objects shows tentative evidence for the Galactic warp, and also exhibits overdensities towards OB associations, clusters, bright rim clouds and the spiral arms of the Galaxy.

The catalogue has been cross-matched with the emission line star catalogue of Kohoutek & Wehmeyer (1999) and also with SIMBAD. We find that a maximum of $\simeq$ 10 per cent of the IPHAS Hα emitters are previously known objects. The SIMBAD matches include several previously known interacting binaries, nebulae and young stellar objects. Many matches are to objects whose detailed classification is unknown, including a sample of infrared, radio and X-ray sources.

ACKNOWLEDGMENTS

Based in part on observations made at the Isaac Newton Telescope, which is operated on the island of La Palma by the Isaac Newton Group in the Spanish Observatorio del Roque de los Muchachos of the IAC. This paper makes use of data obtained at the FLWO Observatory, a facility of the Smithsonian Institution. ARW was supported by a PPARC Studentship. BTG was supported by a PPARC Advanced Fellowship. DS acknowledges a Smithsonian Astrophysical Observatory Clay Fellowship and a PPARC/STFC Advanced Fellowship. PJG is supported by NWO VIDI grant 639.042.201. This research has made use of the SIMBAD database, operated at CDS, Strasbourg, France. This research has made use of NASA's Astrophysics Data System.

REFERENCES

Abraham, P., Dobashi, K., Mizuno, A., Fukui, Y., 1995, A&A, 300, 525
Bronfman, L., 1992, in Blitz, L., ed., The center, bulge, and disk of the Milky Way, vol. 180 of *Astrophysics and Space Science Library*, p. 131
Cichowolski, S., Pineault, S., Arnal, E. M., Testori, J. C., Goss, W. M., Cappa, C. E., 2001, AJ, 122, 1938
Davies, R. D., Elliott, K. H., Meaburn, J., 1976, Mem. R. Astron. Soc., 81, 89
Dennison, B., Simonetti, J. H., Topasna, G. A., 1998, Proc. Astron. Soc. Aust., 15, 147
Dennison, B., Simonetti, J. H., Topasna, G. A., 1999, BAAS, 31, 1455
Drew, J. E., et al., 2005, MNRAS, 362, 753
Freudenreich, H. T., et al., 1994, ApJ, 429, L69
Gaustad, J. E., McCullough, P. R., Rosing, W., Van Buren, D., 2001, PASP, 113, 1326
Haffner, L. M., Reynolds, R. J., Tufte, S. L., Madsen, G. J., Jaehnig, K. P., Percival, J. W., 2003, ApJS, 149, 405
Irwin, M., Lewis, J., 2001, New Astronomy Review, 45, 105
Irwin, M. J., 1985, MNRAS, 214, 575
Kohoutek, L., Wehmeyer, R., 1999, A&AS, 134, 255
Kun, M., Pasztor, L., 1990, Astrophys. Space. Sci., 174, 13
Marschall, L. A., Karshner, G. B., Comins, N. F., 1990, AJ, 99, 1536
Marshall, D. J., Robin, A. C., Reylé, C., Schultheis, M., Picaud, S., 2006, A&A, 453, 635
Mikami, T., Ogura, K., 2001, Astrophys. Space. Sci., 275, 441
Miyamoto, M., Yoshizawa, M., Suzuki, S., 1991, Astrophys. Space. Sci., 177, 399
Odenwald, S. F., Schwartz, P. R., 1993, ApJ, 405, 706
Ogura, K., Sugitani, K., Pickles, A., 2002, AJ, 123, 2597
Russeil, D., 2003, A&A, 397, 133
Shi, H. M., Hu, J. Y., 1999, A&AS, 136, 313
Stephenson, C. B., Sanduleak, N., 1971, Publications of the Warner & Swasey Observatory, 1, 1
University Kyoto, D. O. A., 1982, An atlas of the Northern Milky Way in the h-alpha emission, Contributions from the Department of Astronomy, University of Kyoto, Kyoto: University, Department of Astronomy, 1982
Voges, W., et al., 1999, A&A, 349, 389
Witham, A. R., 2007, , Ph.D. thesis, University of Southampton
Witham, A. R., et al., 2006, MNRAS, 369, 581

This paper has been typeset from a TEX/ LATEX file prepared by the author.